Structural response to O*-O ' and magnetic transitions in orthorhombic perovskites

Aken , van, Bas; Meetsma, A.; Tomioka, Y.; Tokura, Y.; Palstra, Thomas

Link to publication in University of Groningen/UMCG research database

Structural response to O*-O′ and magnetic transitions in orthorhombic perovskites

Bas B. Van Aken,[1] Auke Meetsma,[1] Y. Tomioka,[2,3] Y. Tokura,[2,3,4] and Thomas T. M. Palstra[1,*]

[1]*Solid State Chemistry Laboratory, Materials Science Centre, University of Groningen, Nijenborgh 4, 9747 AG Groningen, The Netherlands*

[2]*Correlated Electron Research Center (CERC), National Institute of Advanced Industrial Science and Technology (AIST), Tsukuba 305-8562, Japan*

[3]*Joint Research Centre for Atom Technology (JRCAT), National Institute of Advanced Industrial Science and Technology (AIST), Tsukuba 305-0046, Japan*

[4]*Department of Applied Physics, University of Tokyo, Bunkyo-ku, Tokyo 113-8656, Japan*

We present a temperature-dependent single-crystal x-ray-diffraction study of twinned orthorhombic perovskites $La_{1-x}Ca_xMnO_3$, for $x=0.16$ and $x=0.25$. These data show the evolution of the crystal structure from the ferromagnetic insulating state to the ferromagnetic metallic state. The data are modeled in space group *Pnma* with twin relations based on a distribution of the *b* axis over three perpendicular cubic axes. The twin model allows full structure determination in the presence of up to six twin fractions using the single-crystal x-ray-diffraction data.

PACS number(s): 61.72.Mm

I. INTRODUCTION

The manganites have generated considerable attention because of the colossal magnetoresistance effect. The role of magnetic order has been widely discussed since double exchange, inducing the ferromagnetic order, is required to generate a metallic ground state. The role of orbital order is much less understood. While *local* Jahn-Teller (JT) distortions are crucial in explaining the localization of the charge carriers in the paramagnetic state, many of the structural features of the *long-range* JT ordering has not been well studied and warrant closer investigation. Even for undoped systems the JT ordering is not well understood as the electronic degrees of freedom have a strong interaction with strain.[1] The orbital ordering in perovskites with degenerate e_g electrons can be easily measured, whereas for degenerate t_{2g} electrons the Jahn-Teller distortions are much smaller. In this paper we focus on the effects of doping on the JT ordering and the role of the lanthanide site shift. In order to minimize the effect of "extraneous" strain, we have studied high-quality single crystals. A method to obtain the crystal structure of twinned orthorhombic samples is presented using single-crystal x-ray diffraction (SXD). Furthermore, we will show how the generally observed *Pnma* symmetry can accommodate a three-dimensional (3D) rotation of the octahedra, known as the GdFeO₃ rotation, concurrently with a Jahn-Teller ordering.

Generally, three basic states for manganites are distinguished, viz. the ferromagnetic metal, the paramagnetic polaronic liquid and the orbital and/or charge ordered antiferromagnetic insulating state. These states can be identified by different structural features. Metallicity induces charge delocalization and is associated with equal Mn-O bond lengths. The charge and/or orbital ordered phases give rise to, for instance, lattice doubling. The polaronic liquid is locally characterized by small polarons.

A method is presented to analyze the 3D twinned crystals, and to apply a full structure determination. Besides it is shown that one does not need a larger data set than for un-

twinned crystals, which is unusual. Using SXD we observe a $2a_p \times 2a_p \times 2a_p$ unit cell, with a_p the lattice parameter of the simple cubic perovskite. It is commonly accepted that the unit cell of $La_{1-x}Ca_xMnO_3$ is $\sqrt{2}a_p \times 2a_p \times \sqrt{2}a_p$. The twinning is unique and it involves a distribution of the *b* axis over three perpendicular cubic axes.[2] This leads to a large fraction, about 25%, of coinciding reflections and an only twice as large unit cell. The observed unit cell originates from a three-dimensional type of twinning that is not restricted to manganites. The model is most likely of general application for a large variety of perovskite *Pnma* crystals.

II. CRYSTAL STRUCTURE

The basic building block of the perovskite structure is a ~ 3.9-Å cubic unit cell with Mn in the center and O at the face centres. The oxygen ions coordinate the Mn ions to form MnO_6 octahedra. The *A* atoms are located at the corners of the cube. The undistorted "parent" cubic structure rarely exists, for instance $SrTiO_3$,[3] but distorts to orthorhombic or rhombohedral symmetry.

A. GdFeO₃ rotation

Due to the small radius of the *A* site ion, with respect to its surrounding cage, the MnO_6 octahedra tilt and buckle to accommodate the lanthanide ion. This is known as the GdFeO₃ rotation[4] and yields the space group *Pnma*. The cubic state allows one unique oxygen position. Due to the GdFeO₃ rotation we need two nonequivalent oxygen positions to describe the structure in *Pnma* symmetry. O2 is the in-plane oxygen, on a general position, (x, y, z). Two opposite Mn-O2 bonds have the same length, but the perpendicular bonds do not need to be equal. O1 is the apical oxygen, located on a fourfold $(x, \frac{1}{4}, z)$ position on the mirror plane. Mn-O1 bonds are always of the same length. Both in the undistorted and the distorted perovskite, the O-Mn-O bond angles are 180° (or near 90°), but due to the buckling
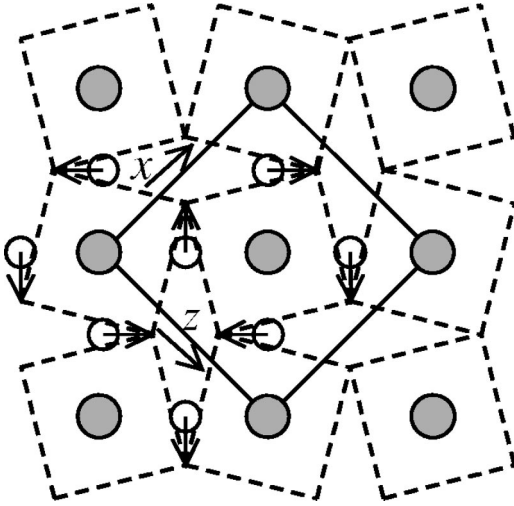
FIG. 1. Sketch of the $GdFeO_3$ rotation in the *ac* plane, obeying *Pnma* symmetry. Mn and O ions are represented by large gray and small open circles, respectively. Open arrows indicate the movement associated with the $GdFeO_3$ rotation. The full line indicates the unit cell.

FIG. 2. Sketch of the $Q2$ JT distortion in the *ac* plane, obeying *Pnma* symmetry. The arrows indicate the movement associated with the JT distortion. The full line indicates the unit cell.

Mn-O-Mn bond angles are significantly less than 180°. A pure $GdFeO_3$ rotation can be obtained within *Pnma* with equal Mn-O bond lengths, as is seen in Fig. 1.

The $GdFeO_3$ rotation is strongly related to the tolerance factor t.[5,6] For an ideal perovskite structure the ratio between the radii of the *A* site ion and the transition-metal ion is such that the tolerance factor is equal to 1. In the La-Ca system the tolerance factor varies from 0.903 to 0.943 going from $LaMnO_3$ to $CaMnO_3$. For the *A* site, a coordination number of nine is assumed, values have been taken from Shannon and Prewitt.[7]

The rotation also depends on the temperature. At high temperature all perovskite structures are (near) cubic, due to the thermal motion of the ions. These motions diminish with decreasing temperature, thereby decreasing the "effective" radius of the ions. As a result, the lanthanides prefer a tighter coordination and this is achieved by an increase in the tilting and buckling of the octahedra.

The rotation is also sensitive to a ferromagnetic ordering. A ferromagnetic ordering is usually accompanied by an increase in the molar volume. For the *Pnma* perovskites, lessening the rotation will yield an increase in molar volume. Therefore, ferromagnetic ordering will be characterized by a step in the rotation parameter, with the smaller rotation in the ferromagnetic phase.

B. Jahn-Teller distortion

The Jahn-Teller effect originates from the degenerate $Mn^{3+}d^4$ ion in an octahedral crystal field. Two possible distortions are associated with the Jahn-Teller effect. $Q2$ is an orthorhombic distortion, with the in-plane bonds differentiating in a long and a short one. $Q3$ is the tetragonal distortion with the in-plane bond lengths shortening and the out-of-plane bonds extending, or vice versa.[8,9] The main result of the distortions $Q2$ and $Q3$ is that the Mn-O distances be-
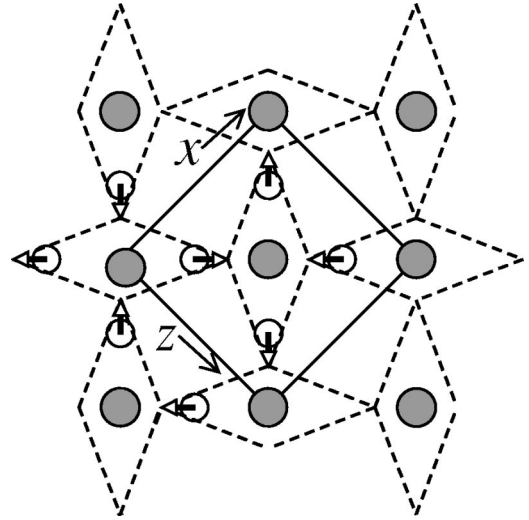
come different and the degeneracy of the t_{2g} and e_g levels is lifted. In Fig. 2, a $Q2$ distortion is shown.

For $LaMnO_3$, the orbital splitting is such that z^2-like orbitals are occupied, alternately oriented along the $x+z$ and $x-z$ axis,[10,11] yielding the $Q2$ distortion. The O2 fractional co-ordinate and this $Q2$ distortion are thus intimately related. For a $Q3$ distortion, only the ratio between the *b* lattice parameter and the *a* and *c* lattice parameters has to change.

C. Oxygen positions

All oxygen positions are related by the symmetry operations of the space group *Pnma*. That means that the in-plane coordinates of one ion (x_{O2}, z_{O2}) determine all other in-plane positions. However, any linear combination of these two parameters and its orthogonal complementary combination will be as good. Normally we prefer x_{O2} and z_{O2}, since we refine the atomic positions as x_{O2} and z_{O2}. However, the oxygen shifts (arrows) in Fig. 1, indicating the rotation, can be expressed as a movement along [1 0 1].[12] We note that these are perpendicular to the oxygen shifts resulting from JT ordering shown in Fig. 2.

Thus, we can express the position of the oxygen atoms relative to their "cubic" position by the "shift" parameters $x_{O2}+z_{O2}$ and $x_{O2}-z_{O2}$ as sketched in Fig. 3. Here, a movement of the O2 ion parallel to [1 0 1],[12] which implies that $x_{O2}+z_{O2}=\frac{1}{2}$, results in equal bond lengths but a Mn-O-Mn angle smaller than 180°. We interpret this movement, along [1 0 1], as the $GdFeO_3$ rotation. Similarly, a shift of the O ion along [1 0 $\bar{1}$], thereby fixing $x_{O2}-z_{O2}=0$, results in different in-plane bond lengths and therefore indicates a Jahn-Teller distortion. The $Q2$ distortion variable is defined as $x_{O2}+z_{O2}-\frac{1}{2}$, thus no distortion yields a $Q2$ distortion parameter equal to zero. The undistorted cubic structure obeys both $x_{O2}+z_{O2}-\frac{1}{2}=0$ and $x_{O2}-z_{O2}=0$. It is clear that any O2 position can be expressed uniquely as a super-position of a $GdFeO_3$ rotation parameter, viz., $x_{O2}-z_{O2}$, and a JT distortion parameter, viz. $x_{O2}+z_{O2}-\frac{1}{2}$.
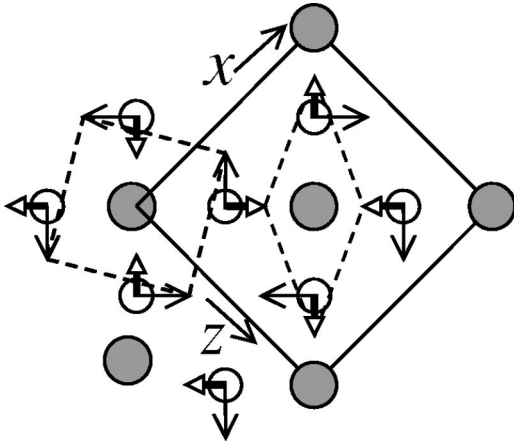
FIG. 3. Sketch of the $GdFeO_3$ rotation (open arrow) and the JT distortion (Δ-arrow) in the ac plane, obeying $Pnma$ symmetry. Mn and O are represented by large gray and small open circles, respectively.

III. STRUCTURE ABO_3 VERSUS IONIC RADIUS

The method of rewriting the oxygen position to two variables, which indicate the magnitude of the JT ordering and the magnitude of the $GdFeO_3$ rotation, is applied to two well-studied series of compounds. Marezio et $al.$ have studied the structure of the $AFeO_3$ single crystals with SXD in great detail.[13] Their data allow us to focus on the correlation between the ionic radius r_A and the magnitude of the rotation. In the top panel of Fig. 4, we see that with decreasing r_A the rotation (open squares) increases monotonously. We also observe an increasing shift from the cubic position for the A site atom with decreasing r_A.

The basic argument favoring the A site shift is that the band-structure energy can be optimised by decreasing the A-O distances for the three shortest bonds and increasing the A-O bond lengths for the three next-shortest bonds. This effect is demonstrated by the cubic-tetragonal transition in WO_3.[15] The tungsten ion is octahedrally surrounded by oxygen ions. Band-structure calculations show that the gap is lowered by a ferroelectric displacement of the W ion off center. The energy is lowered by the overlap between the empty W $5d_{xz}$ and $5d_{yz}$ orbitals with the occupied O $2p_x$ and $2p_y$, respectively.[15]

Goodenough showed the importance of interactions between the A ion, d^0, and the filled oxygen $2p$ orbitals in the case of a $GdFeO_3$ rotation.[16,17] Recently, Mizokawa et $al.$ reported on the interplay between the $GdFeO_3$ rotation, the orbital ordering and the A site shift in ABO_3, with $B = Mn^{3+}$ $(3d^4)$ or V^{3+} $(3d^2)$. Their theoretical calculations suggest that the observed orbital ordering in $LaMnO_3$ is stabilized by both a large $GdFeO_3$ rotation and a shift of the A site ion.[18] Conversely, if a Jahn-Teller distortion is present, then the energy will be lowered if it is accompanied by a shift of the A site.

In cubic perovskites, the A ion is in the center of the AO_{12} polyhedra. The $GdFeO_3$ rotation distorts the AO_{12} polyhedron. Additionally, minimizing the bonding-antibonding energy will decrease the shortest A-O bonds even more by a
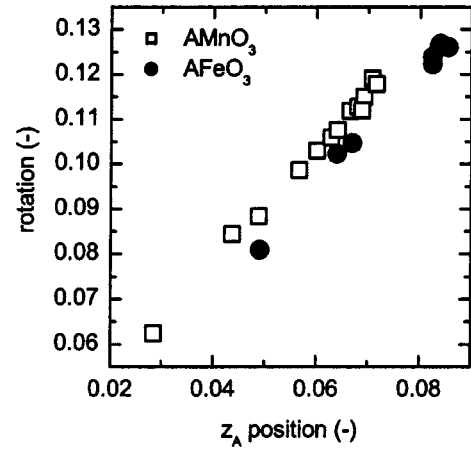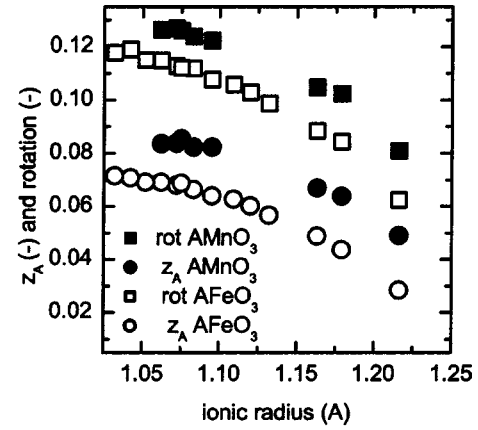

FIG. 4. Top panel: The rotation and z_A vs the ionic radius of $AFeO_3$ and $AMnO_3$. Both parameters indicate a deviation from the cubic perovskite, and both increase with decreasing r_A. Bottom panel: The rotation vs z_A. The parameters show almost perfect correlation indicating their intimate relation. Data have been taken from Ref. 13 ($AFeO_3$) and Ref. 14 ($AMnO_3$). Open and closed symbols represent $AMnO_3$ and $AFeO_3$, respectively. Squares and circles represent the rotation and site shift parameter, respectively.

shift of the A ion. The data of Marezio et $al.$ show the correlation between the rotation and the La site shift.[13] The relevant atomic parameters, x and z (open circles) of the A site, and the rotation parameter (open squares) are fully correlated. The bottom panel shows a perfect linear relation between the A site shift and the rotation parameter of $AFeO_3$ (open symbols). Thus the shift of the A site atom is, in this system, fully determined by the rotation of the FeO_6 octahedron. This conclusion is supported by inspection of the neutron-powder-diffraction (NPD) data on $AMnO_3$ (closed symbols) by Alonso et $al.$[14] Their data show that the JT distortion parameter is $\sim 0.0301(8)$ at $T = 295$ K, independent of the A ion radius.[14] The observed slope of rotation vs site shift is identical for $AMnO_3$ and $AFeO_3$ within the accuracy of the measurement.

The A site shift is the result of the covalent interaction between the A^{3+} ion and the surrounding oxygen ions. The data for $AFeO_3$ show that the ratio $x_A/z_A = 5$. Thus the A ions will decrease their distance to the nearest three oxygen ions by moving along a vector $[1\ 0\ 5]$. As the A coordination

is directly determined by the changes in rotation and distortion, the A site shift strongly depends on both the $GdFeO_3$ rotation and the JT distortion.

Although, thorough structural studies on the manganites are published in the literature, see, e.g., Ref. 19, they typically are based on NPD data of $La_{1-x}Sr_xMnO_3$. In 1971, Elemans *et al.* studied the structure of $LaMnO_3$ and $La_{0.95}Ca_{0.05}MnO_3$, using NPD. They found that the $Q2$ distortion is similar for $T=4.2$ K and $T=298$ K.[11] The Mn-O bond-lengths for $La_{0.75}Ca_{0.25}MnO_3$ are reported by Radaelli *et al.* They show a reduction in the distortion or bond-length disproportion at T_c.[20] Recently, Huang *et al.* report the Mn-O bond lengths for $La_{0.85}Ca_{0.15}MnO_3$, $La_{0.75}Ca_{0.25}MnO_3$, and $La_{0.67}Ca_{0.33}MnO_3$ using NPD. The scatter and error bars make any distinct observation hard. A slight decrease in variance of the bond lengths is observed near T_c.[21] In a Raman study, the MnO_6 distortion was reported to decrease linearly from 42% at $x=0$ to 8% at $x=0.4$, using x-ray powder diffraction.[22] Dabrowski *et al.* studied the relation between oxygen content, doping concentration, and crystal structure for $La_{1-x}Ca_xMnO_3$. They report a transition at room temperature from the O' state, coherent JT distortions, to the $O*$ state at $x=0.14$.[23] No sign of coherent JT distortions was found for $La_{0.8}Ca_{0.2}MnO_3$ and $La_{0.7}Ca_{0.3}MnO_3$ down to $T=15$ K. Increasing the temperature towards T_c, increases the variance in bond lengths, as was determined from total correlation function experiments. This, however, measures the local JT distortions.[24]

IV. EXPERIMENTAL PROCEDURES

The experiments were carried out on single crystals of $La_{1-x}Ca_xMnO_3$, $x=0.16$ and $x=0.25$, obtained by the floating-zone method at Tsukuba, Japan. Although all crystals were twinned, small mosaicity and sharp diffraction spots were observed. Furthermore, sharp magnetic and electronic transitions indicate the good quality of the crystals. A thin piece was cut from the crystal to be used for single-crystal diffractometry. The single crystal was mounted on an ENRAF-NONIUS CAD4 single-crystal diffractometer. The temperature of the crystal was controlled by heating a constant nitrogen flow. Initial measurements were done at 180 K. Temperature-dependent measurements between 90 K and 300 K were performed on a Bruker APEX diffractometer with an adjustable temperature setup. Lattice parameters based on observations by the charge-coupled device camera are refined using all observed reflections. Details of the SXD experiments and refinements are published elsewhere.[25] The single crystals exhibit sharp magnetic transitions with $T_c \sim 160$ K and 200 K, for $La_{0.84}Ca_{0.16}MnO_3$ and $La_{0.75}Ca_{0.25}MnO_3$, respectively.

V. TWINNING

A. The twin structure for manganites

We will focus in this section on the main reason why SXD has not been widely used for these perovskites, namely, twinning. Twinning in doped $LaMnO_3$ originates from the transition of the highly symmetric cubic parent structure to the
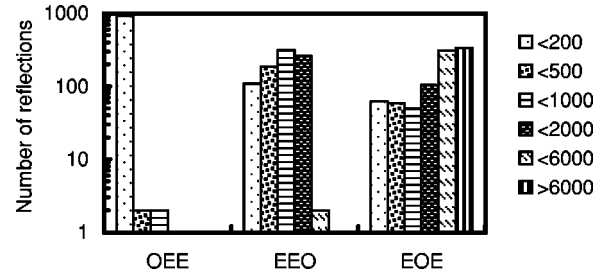

FIG. 5. The number of reflections vs the orientations OEE, EEO and EOE for different intensity ranges. OEE, b' parallel to a'', has mostly very low intensity. Reflections EOE, b' parallel to b'', have a broad range of intensities. In cubic symmetry, these distributions should be identical for absorption corrected data, which we considered.

orthorhombic symmetry, which accommodates both the $GdFeO_3$ rotation and the Jahn-Teller distortion. The solution of the twin relations in the crystals allows us to study in detail the ordering of these compounds as influenced by temperature, magnetic state, and doping concentration. But for now we will focus on the twin relations.

Rodrígruez-Carvajal *et al.* noted that their neutron-powder spectra of pure $LaMnO_3$ could be indexed in a cubic $2a_p \times 2a_p \times 2a_p$ unit cell, above the Jahn-Teller transition temperature.[26] They did not observe an orthorhombic splitting of the peaks. Nevertheless, they could not refine the structure in a cubic unit cell. But full pattern refinement was only possible in the orthorhombic space group $Pnma$.[26] Note that in powder-diffraction data there is no direct method to observe the threefold symmetry along the body diagonal. The refinement has been done in the conventional $Pnma$ setting. They suggested that the powder is twinned but could not give evidence, as they only studied powders. Combining our observation, including the double-cubic lattice, the systematic extinctions and the noncubic intensity distribution, with the suggestion given by Rodrígruez-Carvajal *et al.* leads to the conclusion that our single crystals are twinned.

Electron diffraction and microscopy are instrumental to characterize this twinning because of its high spatial resolution. Recently Déchamps *et al.*[2] identified the twin relations of orthorhombic and rhombohedral $AMnO_3$. Their data are interpreted for $Pnma$ symmetry with coherent domains, with the doubled b axis in three orthogonal orientations.

Reflections in reciprocal space are experimentally observed at a regular distance in three orthogonal directions, corresponding to a cubic lattice spacing of 7.8 Å in real space. Although the three axes had equal lengths, we could not observe the required threefold symmetry axis along $\langle 111 \rangle$ for cubic symmetry. This is shown for EEO reflections in Fig. 5, E denotes an even value for the Miller indices, O stands for odd. Furthermore, studying the intensity distribution of hkl planes with constant h, k, or l showed much regularity, and some anomalous extinction conditions are observed. An overview of these features is given in Appendix A. A twinned structure consisting of coherently oriented $Pnma$ domains is proposed, analogous with the results of Déchamps *et al.*[2] Due to partial overlap this results in a metric cubic system with $a \approx 2a_p \approx 7.8$ Å.

B. Twin model

The transformation of cubic to orthorhombic symmetry requires a designation of a, b, and c with respect to the degenerate cubic axes. There are three possibilities to position the doubled b axis along the three original cubic axes. Thus we propose that the three fractions' b axes are oriented along the three original axes of the cubic unit cell. This twin model consists of a *Pnma* unit cell, transformed by rotation about the cubic [1 1 1] axis. We still have the freedom to choose the a and c axes, perpendicular to the b axis, and rotated 45° with respect to the cubic axes. Therefore, this model yields six different orientations of the orthorhombic unit cell. As the differences between $a/\sqrt{2}$, $b/2$, and $c/\sqrt{2}$ are small, we observe the reciprocal superposition of the six orientations as metrically cubic.

Using the proposed model, the different contributions of the twin fractions to the total integrated peak intensity are taken into account, according to the following procedure. We considered for each observed reflection the corresponding orthorhombic reflections for the twin fractions (if applicable) and used an identical unit cell for each twin. The refined model consisted of the regular parameters in single-crystal diffractometer. This way, both the atomic positions of the asymmetric unit and the volume ratio of the twin domains are refined simultaneously.

Several crystals were measured and refined with this de-twinning model. The refinements showed that for every crystal the distribution of the volume over the twin fractions is different. This is another indication that our crystals are twinned. Other structural deformations than twinning would lead to a constant, not sample dependent, effect on the structure factors. Attempts to refine will then result in the wrong model, giving the same value for the volume fractions, independent of sample. We can also conclude that the size of the twin domains must be smaller than the magnitude of the measured crystals, i.e., 0.1–0.2 mm. Larger twin domains would give rise to crystals of one single domain and even smaller domains are more likely to produce a constant spreading of the domains. Nonregular, though constant, volume fraction of the twin domains could also signal a preferential growth direction of the crystal.

VI. RESULTS

A. Lattice parameters

Reflections in reciprocal space are observed on a double cubic lattice. From these lattice spacings, only the "average" lattice parameters can be calculated. In Fig. 6 the lattice parameter a is plotted against temperature. For $La_{0.84}Ca_{0.16}MnO_3$ the volume fractions of two of the three b axis orientations were very small, therefore, effectively a normal pattern is observed, within only the a-c/c-a twin. For this sample both lattice parameters a and b are plotted. Lattice parameter c behaved identical to lattice parameter a.

The lattice parameter for $La_{0.75}Ca_{0.25}MnO_3$ shows a continuous increase with temperature. No anomaly near T_c can be observed. Lattice parameters a and b for $La_{0.75}Ca_{0.25}MnO_3$, respectively, show a sharp down turn and up turn above $T \sim 250$ K.
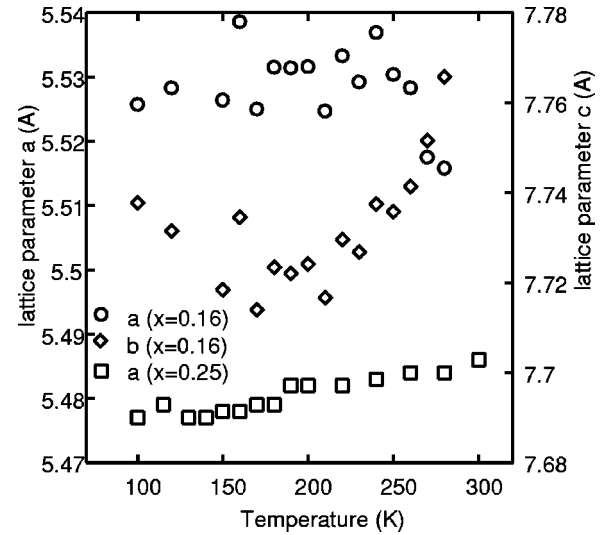

FIG. 6. The temperature dependence of the observed lattice parameters a. For $La_{0.84}Ca_{0.16}MnO_3$ lattice parameter b is plotted on the right axis. The error bars are of the same size as the symbols. Note that the error bars indicate an under limit to the uncertainty.

B. Rotation

In Fig. 7 the temperature dependence of the rotation is plotted vs the temperature. The rotation-temperature curves depend strongly on the Ca concentration. The curve of the $x = 0.25$ sample shows a sharp steplike increase in the rotation at T_c. At $x = 0.16$, the scatter in the data is larger, though a smaller step near T_c can still be observed. Above T_c, the rotation decreases with a similar slope as the curve for $x = 0.25$. The absolute value of the rotation is about 10% larger for the lower-doped sample.

C. JT distortion parameter

Figure 8 shows that the sample with $x = 0.16$ has a constant value for the JT distortion parameter at low temperature. Above $T = 260$ K the JT distortion parameter decreases rapidly with temperature, which signals the JT orbital ordering temperature.

The JT distortion parameter for the $x = 0.25$ sample is independent on temperature within the uncertainty of the ex-
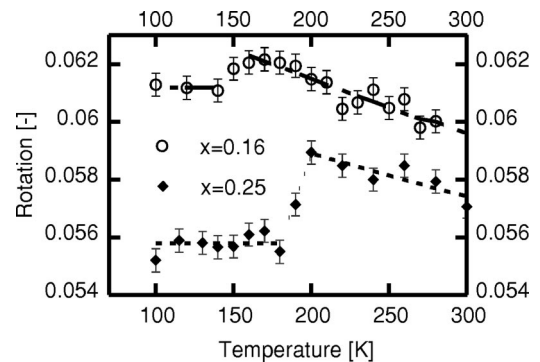

FIG. 7. The temperature dependence of the rotation parameter. The broken lines are guides to the eye.
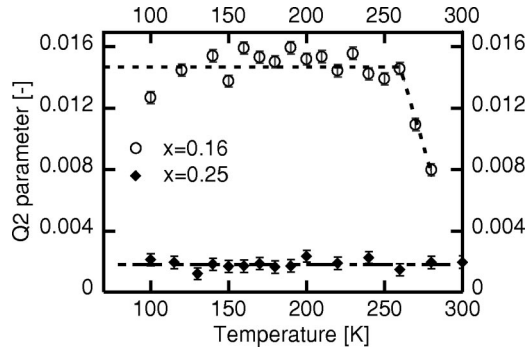
FIG. 8. Jahn-Teller parameter against temperature. The broken lines are guides to the eye.

periment. The value of 0.002 results from the fact that the O2 position is not constrained by symmetry.

D. La site shift

In Fig. 9, we show the temperature dependence of the A position, $(x_A, \frac{1}{4}, \frac{1}{2} - z_A)$, with respect to the ideal position $(0, \frac{1}{4}, \frac{1}{2})$. We note that the error bars of the A position, 0.0001, and scatter are much smaller than the error bars on the JT distortion parameter and rotation parameter, 0.0005. These latter are derived from the oxygen positions, which have a larger uncertainty due to their smaller electron density.

The ratio of x_A and z_A is constant, with x_A roughly five times larger than z_A for all temperatures.

VII. DISCUSSION

A. Lattice parameters

The occurrence of twins in our single crystals effectively averages the lattice parameters a, b, and c, since reflections with different hkl, originating from different twin fractions, coincide in one reflection spot. However, for the $x=0.16$ sample, only twin fractions with parallel b axes are observed, which allows a separate determination of a/c and b. The lattice parameter c is still averaged with a.

The lattice parameters, or volume of the unit cell, are influenced by several effects. The most obvious in a temperature-dependent study is the thermal expansion. We clearly observe the continuous increase in lattice parameter a with temperature for $x=0.25$. The GdFeO$_3$ rotation is another nonvolume conserving distortion of the lattice. The main reason the MnO$_6$ octahedra are rotated is the ionic

radius of the A site atom. We expect a change of volume at T_c, but we could not observe an anomaly in the lattice parameters at $T=200$ K ($x=0.25$) or at $T=160$ K ($x=0.16$).

An orbital ordering can have an effect on the lattice parameters, even though it is volume conserving. The effect is different for the $Q2$- and $Q3$-type distortion. The coherent $Q2$ distortion does not change the lattice parameters in first approximation as the long and short Mn-O bonds are oriented alternately, both in the $[1\,0\,1]$ and the $[1\,0\,\bar{1}]$ direction. However, the $Q3$ distortion has a significant effect on the lattice parameters. Because it has an opposite effect on the Mn-O1 bonds, parallel to b, and the Mn-O2 bonds, in the ac plane.

Note that there is a large scatter in Fig. 6. Combined with the averaging effect of the twin domains, the responses of the crystal structure to the orbital ordering or the ferromagnetic transitions are not very clear. This stresses the importance of an alternative way to study the relation between the structure and the electronic properties.

B. Rotation

The rotation parameter is clearly sensitive to the ferromagnetic ordering in the $x=0.25$ samples at $T_c=200$ K. Likewise a smaller transition is shown in the $x=0.16$ curve in Fig. 7. The decrease in rotation parameter indicates a straightening of the Mn-O-Mn bond angles as shown in Fig. 1 and the text. If a constant volume of the MnO$_6$ octahedra is assumed, the decrease in rotation, associated with the paramagnetic to ferromagnetic transition, yields an increase in total volume. An increase in molar volume, or an increase in the lattice parameters is a common feature of ferromagnetic ordering, as observed for instance in pure nickel.[27] This agrees very well with our observation of the decreasing rotation parameter and consequently increasing volume of the unit cell.

The rotation for LaMnO$_3$ is 0.0810(2) at room temperature and decreases with temperature.[26] Elemans *et al.* reported no significant change in rotation between room temperature and 4.2 K, but their resolution is smaller. However, by doping with 5% Ca a decrease in the rotation parameter to 0.077(1) is observed.[11] Ca MnO$_3$ is (almost) cubic and consequently has no rotation. Therefore, we expect a continuous decrease in the rotation with increasing doping. This agrees well with our data, which show a decrease of the absolute value of the rotation with 5–10 % between $x=0.16$ and $x=0.25$.
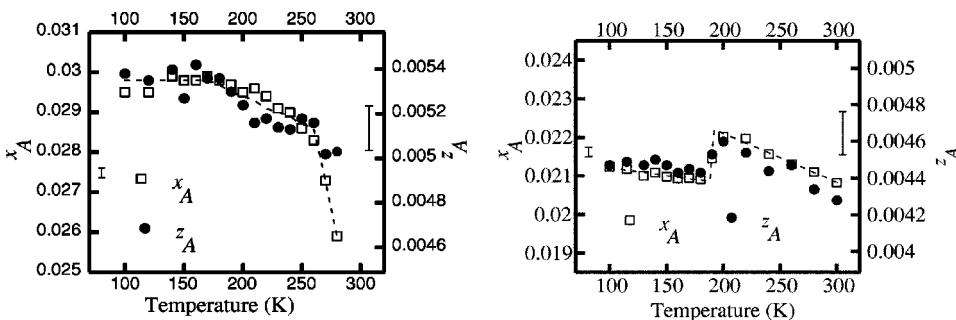
FIG. 9. The temperature dependence of the A site position of La$_{0.84}$Ca$_{0.16}$MnO$_3$ (left) and La$_{0.75}$Ca$_{0.25}$MnO$_3$ (right). The ratio between x_A and z_A is 5.6 and 4.8. The x_A axes have the same scale to allow comparison. The corresponding z_A axes have been scaled with the average ratios 5.6 and 4.8.

C. JT distortion parameter

In Fig. 8, we observe that the $Q2$ distortion for the $x = 0.25$ sample is constant with temperature, but not equal to zero as expected for the ferromagnetic metallic phase. The value, 0.002(1), is in good agreement with values calculated from structure determinations of AFeO$_3$, e.g., 0.0036 for LuFeO$_3$.[13] Fe $3d^5$ in the high-spin state, has a completely filled subband, and is therefore not sensitive to the JT effect. However, other effects, for example, related to the hybridization associated with the A site shift, and the degrees of freedom of the O2 position in *Pnma* symmetry allow the $Q2$ distortion to be nonzero.

The reduction in $Q2$ parameter, as shown by the curve for $x = 0.16$, clearly coincides with the JT ordering temperature. As single-crystal diffraction is sensitive to long-distance correlations, this either means that the orbitals become disordered or that there is an overall reduction in the magnitude of the local $Q2$ distortion. Local probes, such as pair distribution functions, show that even in the paramagnetic phase the local distortions do not disappear.[28] Our observation of a decrease in $Q2$ distortion is therefore caused by a decrease in the coherence of the orbital order.

The data for LaMnO$_3$ show that the JT distortion parameter is about 0.0320(10) at room temperature and that the JT ordering reduces to 0.0060 at $T = 798$ K, where the orbital order is known to disappear.[26,29] The low-temperature JT distortion parameter and the JT transition temperature strongly depend on the doping level, x. With increasing doping both variables decrease.

D. La site shift

The ratio of x_A and z_A corresponds to a shift of the A atom along [1 0 5]. Mizokawa *et al.* assumed the A site shift along [1 0 7].[18] Their assumed [1 0 7] is in good agreement with our experimental observation of [1 0 5].

In Fig. 9, changes in the gradient are observed near T_c and the orbital ordering temperature, corresponding with the step in the resistance curve. This supports the assumption that the A site shift is sensible to changes in the oxygen environment, by changes in the GdFeO$_3$ rotation and the JT distortion.

The A site shift, expressed by x_A, in LaMnO$_3$ is 0.0490(2) at room temperature and 0.0217(3) at 798 K.[26] The latter value is comparable with the observed values near 300 K for $x = 0.25$.

If we compare these curves with the curves in Figs. 7 and 8 it is obvious that the curve of rotation vs temperature of the $x = 0.25$ sample is mimicked by the A site shift vs temperature curve. Similarly, the A site shift vs temperature curve of the $x = 0.16$ sample shows the same rapid fall above $T = 260$ K as the curve of the JT distortion parameter vs temperature. But a small change in slope is observed at T_c. Evidently the A site shift is a good probe to pinpoint transitions which involve changes in the oxygen coordination of the Mn ions.

VIII. CONCLUSION

We conclude that full structure determination using single-crystal x-ray diffraction provides accurate information
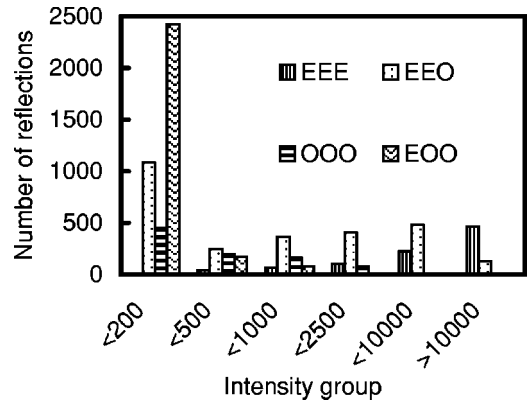

FIG. 10. The intensity distribution of reflections. Low intensities, $I < 200$ are mostly EOO, while high intensities, $I > 2500$, are of the types EEE and EEO, E denotes an even value for the Miller indices, O stands for odd.

regarding the magnetic and orbital ordering in manganite perovskites. We showed that the twinning of these single crystals is based on a distribution of the doubled b axis over three perpendicular cubic perovskite axes. The shift of the A site atoms is very sensitive to changes in the oxygen environment of the A site. Therefore, the A site shift is an accurate probe for magnetic transitions and orbital ordering, since these involve rotations and deformations of the MnO$_6$ octahedra network. This warrants structure investigations close to the ferromagnetic insulator to ferromagnetic metal transition near $x = 0.2$.

APPENDIX A: DATA ANALYSIS

Although cubic symmetry could not be observed, some regularities and anomalous extinction conditions are present in the intensity distribution over hkl space. In Fig. 10 the observed intensity distribution of the reflections is plotted. The reflections are subdivided in four groups, on the basis of the number of odd indices in the double-cubic setting. Here the effect of the twin model on the visibility of the standard *Pnma* reflection conditions is described and a detailed analysis of the intensity distribution of a model crystal with *Pnma* symmetry and of the measured reflections in double-cubic setting is given. The first step in space-group determination is to search for systematic absences in the list of reflections. We observe no intensity for the reflections shown in Table I. Note that the indices are in double-cubic setting and therefore allow cyclic permutation, i.e., $h00$, $0k0$, and $00l$ are all represented by $h00$. These reflection conditions only allow the space groups $P2_13$ and $P4_232$. Attempts to determine the structure using these space groups were unsuccessful. But, these space groups only have $h00$: $h = 2n$ as reflection

TABLE I. Extinct reflections as observed in the $2a_p \times 2a_p \times 2a_p$ data set.

Reflection	Extinction condition	Observed reflections
$h'' \ 0 \ 0$	$h \neq 2n$	E00[30]
$h'' \ \overline{h''} \ 0$	$h \neq 2n$	EE0[30]
$h'' \ k'' \ h''$	$h \neq 2n, k = 2n$	EOE[30]
$h'' \ k'' \ \overline{h''}$	$h \neq 2n, k = 2n$	EOE[30]

condition. This suggests that we have more information than can be attributed to these space groups. Furthermore, the observed and, for cubic systems, anomalous reflection conditions suggested that we might be looking at a twinned crystal. In the next paragraph, we present the transformation of the reflection conditions for orthorhombic *Pnma* according to the presented twin model.

The following equations are used to transform the simple-cubic Miller indices hkl to the standard *Pnma* setting and to transform these to the double-cubic setting.

$$h',k',l' = h+l, 2k, -h+l, \quad (A1)$$

$$h'',k'',l'' = h'-l', k', h'+l'. \quad (A2)$$

The reflection conditions for *Pnma* are shown in Table (II). Using Eq. (A2) the *Pnma* reflection condition $0 \ k' \ 0$: $k' = 2n$ is transformed to double-cubic as $0 \ k'' \ 0$: $k'' = 2n$ and with cyclic permutation yielding $h'' \ 0 \ 0$: $h'' = 2n$ and $0 \ 0 \ l''$: $l'' = 2n$. This corresponds to the reflection condition $h'' \ 0 \ 0$: $h'' = 2n$ in Table I. However, *Pnma* reflections of the type $h' \ 0 \ h'$ are also transformed to $h'' \ 0 \ 0$, with $h'' = 2h'$. Note that the orthorhombic to double cubic transformation gives $0 \ k' \ 0 = h'' \ 0 \ 0$, with $b' \| a''$, and the reflection condition $k' = 2n$ implies that only $h'' = 2n$ are present. While the $h' \ 0 \ h'$ reflections intrinsically give $h'' \ 0 \ 0$ with $h'' = 2n$, with $b' \| b''$. This implies that $h' \ 0 \ h'$ may never contribute intensity to reflections $h'' \ 0 \ 0$, with h'' odd. Conversely, if we do not observe intensity on reflections $h'' \ 0 \ 0$: $h'' \neq 2n$, then all of the constituting *Pnma* reflections, at most six, should be absent.

To transform and understand the other reflection conditions of *Pnma* we have to take into account that an orthorhombic, and also a cubic, unit cell implies that hkl is equivalent upon sign reversal of each of the Miller indices. The *Pnma* reflection condition $h' \ 0 \ 0$: $h' = 2n$ becomes $h'' \ 0 \ h''$: $h'' = 2n$ and similarly $0 \ 0 \ l'$ transforms to $\overline{l''} \ 0 \ l''$. But as we just stated, $h'' \ 0 \ h''$ is identical to $\overline{h''} \ 0 \ h''$. If we combine reflections then a reflection condition is fulfilled if any of the contributing parts has intensity. To obtain extinction, all con-

TABLE II. Reflection conditions for space group *Pnma*.

$0kl$	:	$k+l=2n$
$0k0$	:	$k=2n$
$00l$	:	$l=2n$
$hk0$	:	$h=2n$
$h00$	:	$h=2n$

tributing reflections should be extinct. As $0 \ 0 \ l'$ has no extinction condition, i.e., intensity for all l', they will contribute to all $h'' \ 0 \ h''$ / $\overline{h''} \ 0 \ h''$ reflections, and the *Pnma* reflection condition $h' \ 0 \ 0$: $h' = 2n$ is masked.

The overlap of different reflections also occurs for $0 \ k' \ h'$ and $h' \ k' \ 0$. These transform to $\overline{h''} \ k'' \ h''$ and $h'' \ k'' \ h''$. Therefore, we cannot disentangle $0 \ k' \ h'$ and $h' \ k' \ 0$ in the measured double-cubic cell. The *Pnma* reflection conditions for $0 \ k' \ l'$ and $h' \ k' \ 0$ are $k' + l' = 2n$ and $h' = 2n$, respectively. $h'' \ k'' \ h''$ and $h'' \ k'' \ \overline{h''}$ are found to be extinct for $h'' \neq 2n$ and $k'' = 2n$ in the double-cubic setting. To have these reflections extinct, all contributing *Pnma* reflection conditions must be extinct. This implies that *both $h' = 2n$ and $k' + h' = 2n$*, which are the reflection conditions for the contributing $0 \ k' \ h'$ and $h' \ k' \ 0$, may not be fulfilled. Thus, taking into account that $h'' = h' + 0$ and $k'' = k'$, it is easily derived that $h'' \neq 2n$ and this yields $k'' = 2n$. This means OEO reflections are extinct.

Now we consider reflections of the type $h'' \ k'' \ h''$ that are not extinct. Our twin model yields six fractions that can contribute to the considered reflections.

(1) $h'' = 2n$ and $k'' = 2n$. Reflections EEE have contributions from the four fractions with the doubled b' axis parallel to either a'' or c'', this is also true for reflections OOO. In addition, we have contributions from the two fractions with b' parallel to b'', i.e., from $h' \ k' \ 0$ and $0 \ k' \ h'$.

(2) $h'' \neq 2n$ and $k'' \neq 2n$. Reflections OOO, in addition to the four fractions with the doubled b' axis parallel to either a'' or c'', have one additional contribution from $0 \ k' \ h'$. In the special case that $h'' = k''$, for both EEE and OOO, then two of the four fractions, parallel to a'' and c'' contribute.

(3) $h'' = 2n$ and $k'' \neq 2n$. Reflections EOE, only have a contribution from the $h' \ k' \ 0$ reflection, with b' parallel to the observed b'' axis.

We have shown that the intensity of observed $h'' \ k'' \ h''$ reflections depends on odd or even. We conclude that $h'' \ k'' \ h''$ reflections are extinct for OEO, while the other reflections have contributions from up to six twin fractions.

We can also learn something about the twinned origin by studying the intensity distribution. Our twin model provides a natural explanation for the hierarchy in intensities of the reflections. First, we consider the known transition from the single-cubic unit cell to the orthorhombic one to elucidate the patterns that are inherent to perovskites. Then we proceed to show how these patterns are convoluted in the double-cubic, twinned model.

The intensity distribution of a normal *Pnma* perovskite is shown in Fig. 11. In conventional orthorhombic *Pnma* the reflections $h' \ k' \ l'$ with $h' + l' = 2n$ are stronger than $h' + l' \neq 2n$. From these, the $k = 2n$ reflections are stronger than the $k \neq 2n$ ones. This can be attributed to their origin in the 3.9 Å cubic structure. The $h' \ k' \ l'$ reflections in orthorhombic setting originate from hkl in the single-cubic cell according to Eq. (A1). Therefore, h' and l' will always be both even or both odd if the reflection $h' \ k' \ l'$ is related to an integer single cubic crystal plane. In other words if $h' + l' \neq 2n$ then the reflections originate from a crystal plane in the single cubic setting with a noninteger Miller index,
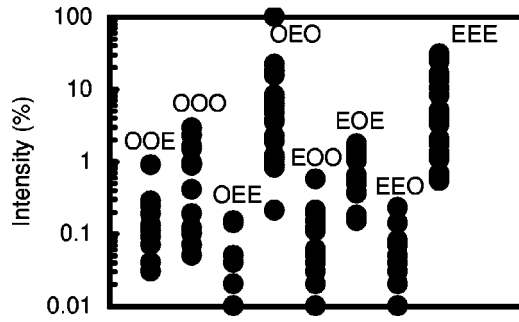
FIG. 11. The calculated intensities for a conventional perovskite, subdivided with respect to odd and even of the Miller indices. $k=2n$ reflections are strongest, if $h'+l'=2n$. Reflections with $h'+l'\neq 2n$ have roughly 100 times less intensity.

i.e., a superlattice reflection and their intensities are typically weak. The same argument can be applied to k. As $k'=2k$, reflections with $k'=2n$ originate from a regular crystal plane and reflections with $k'\neq 2n$ are superlattice reflections. These reflections with $k'\neq 2n$, however, appear to have somewhat more intensity than the $h'+l'\neq 2n$ reflections.

We observe the following patterns in the intensity distribution of the double cubic cell. First, reflections EEE are generally the strongest, EOO (Ref. 30) usually absent, or very weak. The following hierarchy can be made if we disregard the cubic symmetry. EOE reflections were much stronger than EEO, which are again stronger than OEE. Likewise, OEO reflections were, although weak, stronger than OOE and again stronger than EOO.

In conventional *Pnma* structure we found that if $h'+l' \neq 2n$ then reflections with $k'\neq 2n$ are stronger than those with $k'=2n$. In our even/odd notation, for the *Pnma* structure this yields (EEE=OEO)≫(OOO=EOE)≫(OOE =EOO)≫(OEE=EEO). So there are roughly four intensity groups. We can correlate these four groups with the four types of reflections we measured in the supercubic setting, with the following intensity hierarchy: EEE≫EEO≫OOO ≫EOO. Here we consider the transformation from the orthorhombic to the double-cubic setting for the in-plane indices, h' and l'. Double-cubic indices are calculated with $h'+l'$ and $h'-l'$, therefore h'' and l'' will be both even or both odd. Reflections of the type E?O or O?E will have no intensity of the twin with b' parallel to b'', as they are not originating from an ''integer'' crystal plane. In contrast with the single-cubic to orthorhombic *Pnma* transition, where orthorhombic superlattice reflections are allowed, the orthorhombic to double-cubic transformation is just a new choice of reference system, that may not and cannot generate new reflections. But we have a mixing of different orientations of the b' axis along the three cubic axes a'', b'', and c'', which do generate reflections where none are observed without the twinning. We can cycle the indices of these reflections so that we get either E?E or O?O. From the corresponding twin, with b' parallel to either a'' or c'', we do have intensity on these E?O and O?E reflections. EOE and OEO will only have contributions from this particular setting with $b'\|b''$. EEE and OOO can be cycled and in general have contributions from all six orientations.

1. Intensity

The small deviations from the cubic symmetry are reflected in the intensities of the reflections. To illustrate this point, we transform an arbitrary, subcell, reflection hkl to the orthorhombic setting by Eq. (A1). Thus orthorhombic reflections with k' even and h' and l' both even or both odd stem from planes that already existed in the original cubic unit cell. We observe in all diffraction patterns of orthorhombic perovskites that reflections that originate from cubic crystal planes generally have higher intensities than those have that do not.

The intensity of a particular twin fraction is proportional to the volume of that twin fraction. Using the uniqueness of some reflections, i.e., belonging to only one twin fraction lattice, we can search for the orientation of the largest fraction. All b' axes are oriented along one of the measured double-cubic axis. It is impossible to differentiate the two fractions with parallel b' and perpendicular a' and c'. We considered groups of reflections with cycled indices, having either one odd, OEE, or one even index, EOO. Roughly, the intensities of the reflections within these groups occurred with ratio 70:20:10. This suggested that one twin had 70% of the volume, the others 20% and 10%.

These reflections are sorted to find the corresponding orientations. The sort parameter is the observed double-cubic axis that corresponded with the odd indices in OEE, and the even indices in EOO. Only cycled reflections that occurred three times with measurable intensity were taken into account. We found that $I_{a''}:I_{b''}:I_{c''}=5:80:15$. The constraint that all three intensities have positive values ignores the weakest reflections. This method also ignores Bijvoet pairs, as we only measured $-20<l''<2$. In principle EOO and $\overline{EOO}$ should have identical intensity. If we indeed had a cubic system then these variations should be zero within standard deviation. The distribution of the intensities, with respect to the different axes, strongly suggests that the crystal is twinned.

2. Intensity distribution

Careful analysis of the intensity distribution shows extra evidence for the proposed models. Two important observations are made. First, the full data set shows that reflections hkl of type EEE are by far the strongest. Second, reflections having one odd Miller index, OEE, EOE nband EEO, are second strongest in intensity. Of these reflections EOE has the highest intensity as seen in Fig. 5.

To understand the observed intensity distribution in the $2a_p\times 2a_p\times 2a_p$ unit cell, we examine the influence of the structural deformations on the structure factors. Despite the effect of Jahn-Teller distortions, $GdFeO_3$ rotations and twinning the structure remains in origin cubic. This means that the intensity distribution of the peaks with high intensity will always mimic the intensity distribution of the peaks of the undistorted cubic perovskite. An arbitrary reflection, in the small cubic subcell, hkl, is transformed to the orthorhombic unit cell using Eq. (A1) Thus orthorhombic reflections with h' and l' both even or both odd and k' even stem from the original cubic unit cell. These reflections therefore have the

highest intensity, see Fig. 11. Although the fact that the h' k' $l'=$EOE reflections do not originate from the original cubic planes, they are allowed in the *Pnma* symmetry. In Table II the reflection conditions for the *Pnma* space group are given. Extinctions observed in the double-cubic setting are thoroughly discussed before. Reflections h' k' l' that satisfy the condition h' k' $l'=$EOE have higher intensities than those that do not.

With these observations, we return to the observed double-cubic lattice. To double the *Pnma* unit cell to a $2a_p \times 2a_p \times 2a_p$ unit cell, a reflection h' k' l' is transformed to h'' k'' l'' using Eq. (A2). The transformation yields that double cubic reflections with $k''=2n$, $k''=k'$, originate from single cubic reflections with $k=n$. Likewise, $k''=2n+1$ reflections originate from noninteger single cubic indices k, and will therefore have less intensity. This explains why the measured $h''k''l''=$EEE reflections are strongest and EOE are one order of magnitude less strong.

We have seen that $h''=h'-l'$ and $l''=h'+l'$ thus h'', and l'' are always both even or both odd. Therefore, EOE only has contributions of the fractions with k'' corresponding to the orthorhombic *b* axis. OEE and EEO originate from fractions with their *b* axis parallel to a'' and c'', respectively. The fact that our observed EOE is stronger than OEE and EEO, indicates that, by chance, the observed b'' axis is parallel with the b' axis of the largest twin fraction.

3. Refinement

Both the Ca content and the volume fractions of the twins can be determined from single-crystal x-ray diffraction in the following way. First a full hemisphere of reciprocal *hkl* space is measured. On this very large data set, the atomic positions, the Ca content, and the volume fractions are refined. The results of the refinement are compared with a refinement on only one octant of these measured reflections. The outcome was equivalent within the error bars. We refined again fixing the twin fractions and Ca concentration to the values found for the first refinement on the large data set, and allowing only the atomic coordinates and anisotropic displacement parameters to change. This resulted in the same structural model as found with the complete structure determination on the largest data set.

It is concluded that apparently the refinement is insensitive for the size of the data set. However, it will be dependent on the θ range of the data set. The insensitivity can be understood if we view the symmetry relations and Friedel pairs. Due to the Patterson symmetry, *mmm*, the relation $F(\bar{h}kl)=F(hkl)$ is valid for all structure factors. Friedel pairs are reflections that have intrinsically the same structure factor, related thus by symmetry and ignoring absorption and anomalous scattering effects. Although we have six different orientations, one octant chosen in a particular orientation will still contain data of all fractions. The six orientations can be transformed in such a way that every h' k' l' is represented for all three *b* directions in one octant of reciprocal space.

APPENDIX B: IMPLEMENTATION IN REFINEMENT

The standard refining programs can work with twin models, but only if they consist of merohedral twins. In our case,

the reflections do not correspond with an orthorhombic unit cell, but with a, twice as large, pseudocubic unit cell. Here we will explain the way we worked around the refining program.

First, a hemisphere in *hkl* space was measured with $-20<h<20$, $-20<k<20$ and $0<l<20$. On this data set, we could refine our twin model with the six fractions, including the Ca concentration on the *A* site. Measuring such a large range in *hkl* space requires a large amount of time, roughly ten days in the present setup. Typically, for crystals with an orthorhombic unit cell measuring one octant of reciprocal space is sufficient. From refinements on selected parts of the data set, we concluded that we could investigate the structure, for instance at different temperatures, by measuring only the positive octant of the main fraction, thereby considerably limiting the measuring time.

Here we describe the model and the application by SHELXL. The standard refining programs can work with merohedral twin models. However, in our case, the observed lattice does not coincide with one orthorhombic unit cell. Every observed reflection has contributions of up to six twin fractions. We measured both in the double-cubic setting as in the orthorhombic setting of the main twin fraction. We transformed the $h''k''l''$ indices to the six possible twin orientations by

$$h',k',l' = \frac{1}{2}(k''+l''), \quad h'', \quad \frac{1}{2}(k''-l'')$$

$$\text{and } \frac{1}{2}(k''-l''), -h'', \frac{1}{2}(k''+l''), \quad \text{(B1)}$$

$$h',k',l' = \frac{1}{2}(h''+l''), \quad k'', \quad \frac{1}{2}(-h''+l'')$$

$$\text{and } \frac{1}{2}(-h''+l''), -k'', \frac{1}{2}(h''+l''), \quad \text{(B2)}$$

$$h',k',l' = \frac{1}{2}(-h''+k''), \quad l'', \quad \frac{1}{2}(h''+k'')$$

$$\text{and } \frac{1}{2}(h''+k''), -l'', \frac{1}{2}(-h''+k''), \quad \text{(B3)}$$

A new software program TWINSXL was developed to transform the standard data file, HKLS, by using the appropriate transformation matrices from a second input file.[31] The new data file is constituted of lines of h',k',l', intensity plus standard deviation and twin fraction number. We used the "HKLF 5" option of SHELXL to refine data. The refinement uses a crystal model for the orthorhombic structure with the normal, adjustable variables. Five variables for the twin fractions were added, the sixth fraction is calculated as the complement of the other five fractions. The sum of the appropriate calculated intensities for all fractions was compared with the observed integrated intensities.

*Electronic address: palstra@chem.rug.nl

[1] N.D. Mathur and P.B. Littlewood, Solid State Commun. **119**, 271 (2001).

[2] M. Dechamps, A.M.D. Guevara, L. Pinsard, and A. Revcolevschi, Philos. Mag. A **80**, 119 (2000).

[3] A. von Hippel, R. Breckenridge, F.G. Chesley, and L. Tisza, Ind. Eng. Chem. **38**, 1097 (1946).

[4] The GdFeO$_3$ rotation comprises only of rotating MnO$_6$ octahedra. The term ''GdFeO$_3$ rotation'' will be used here. Distortion is restricted to the ''*Jahn-Teller distortion*.''

[5] V.M. Goldschmidt, Fortschr. Mineral. **15**, 73 (1931).

[6] V.M. Goldschmidt, Handwörterb. Naturwiss. 2. Aufl. **5**, 1128 (1934).

[7] R.D. Shannon and C.T. Prewitt, Acta Crystallogr., Sect. A: Cryst. Phys., Diffr., Theor. Gen. Crystallogr. **32**, 751 (1976).

[8] J. Kanamori, J. Appl. Phys. **31**, 14S (1960).

[9] Y. Yamada, O. Hino, S. Nohdo, R. Kanao, T. Inami, and S. Katano, Phys. Rev. Lett. **77**, 904 (1996).

[10] J.B. Goodenough, Phys. Rev. **100**, 564 (1955).

[11] J.B.A.A. Elemans, B. van Laar, K.R. van der Veen, and B.O. Loopstra, J. Solid State Chem. **3**, 238 (1971).

[12] The O2 position, (x_O2, y_O2, z_O2) near ($\frac{1}{4}$,0,$\frac{1}{4}$) is used here. The other three oxygen positions in the same xz plane of the unit cell follow from the space-group symmetry. For these the shifts are also transformed according to the symmetry operations.

[13] M. Marezio, J. Remeika, and P. Dernier, Acta Crystallogr., Sect. B: Struct. Crystallogr. Cryst. Chem. **26**, 2008 (1970).

[14] J. Alonso, M. Martez-Lope, M. Casais, and M. Fernández-Díaz, Inorg. Chem. **39**, 917 (2000).

[15] G.A. de Wijs, P.K. de Boer, R.A. de Groot, and G. Kresse, Phys. Rev. B **59**, 2684 (1999).

[16] J.B. Goodenough, *Magnetism and the Chemical Bond* (Wiley, New York, 1963).

[17] J.B. Goodenough, Prog. Solid State Chem. Phys. Rev. **5**, 145 (1971).

[18] T. Mizokawa, D.I. Khomskii, and G.A. Sawatzky, Phys. Rev. B **60**, 7309 (1999).

[19] B. Dabrowski, X. Xiong, Z. Bukowski, R. Dybzinski, P. Klamut, J. Siewenie, O. Chmaissem, J. Shaffer, C. Kimball, and J. Jorgensen, Phys. Rev. B **60**, 7006 (1999).

[20] P.G. Radaelli, M. Marezio, H.Y. Hwang, S.-W. Cheong, and B. Batlogg, Phys. Rev. B **54**, 8992 (1996).

[21] Q. Huang, A. Santoro, J.W. Lynn, R.W. Erwin, J.A. Borchers, J.L. Peng, K. Ghosh, and R.L. Greene, Phys. Rev. B **58**, 2684 (1998).

[22] E. Liarokapis, T. Leventouri, D. Lampakis, D. Palles, J.J. Neumeier, and D.H. Goodwin, Phys. Rev. B **60**, 12 758 (1999).

[23] B. Dabrowski, R. Dybzinski, Z. Bukowski, O. Chmaissem, and J. Jorgensen, J. Solid State Chem. **146**, 448 (1999).

[24] S.J. Hibble, S.P. Cooper, A.C. Hannon, I.D. Fawcett, and M. Greenblatt, J. Phys.: Condens. Matter **11**, 9221 (1999).

[25] B.B. Van Aken, Ph.D. thesis, University of Groningen 2001, www.ub.rug.nl/eldoc/dis/science

[26] J. Rodríguez-Carvajal, M. Hennion, F. Moussa, A.H. Moudden, L. Pinsard, and A. Revcolevschi, Phys. Rev. B **57**, R3189 (1998).

[27] C. Williams, Phys. Rev. **46**, 1011 (1934).

[28] S.J.L. Billinge, R.G. DiFrancesco, G.H. Kwei, J.J. Neumeier, and J.D. Thompson, Phys. Rev. Lett. **77**, 715 (1996).

[29] Y. Murakami, J.P. Hill, D. Gibbs, M. Blume, I. Koyama, M. Tanaka, H. Kawata, T. Arima, Y. Tokura, and K. Hirota, Phys. Rev. Lett. **81**, 582 (1998).

[30] We do not explicitly mention the different orientations of the orthorhombic unit cell. If the regarded b axis is not parallel with b'', than the indices should be cycled appropriately.

[31] A. Meetsma, Computer code TWINSXL (University of Groningen Groningen, 2000).